

Heterogeneous & Homogeneous & Bio- & Nano-

CHEM **CAT** CHEM

CATALYSIS

Accepted Article

Title: Synthesis of ZnO nanoparticles assisted by N-sources and their application in the photodegradation of organic contaminants

Authors: Gelson T. S. T. Silva, Kele T. G. Carvalho, Osmando F. Lopes, Eliziana S. Gomes, Andréa R. Malagutti, Valmor R. Mastelaro, Caue Ribeiro, and Henrique A. J. L. Mourão

This manuscript has been accepted after peer review and appears as an Accepted Article online prior to editing, proofing, and formal publication of the final Version of Record (VoR). This work is currently citable by using the Digital Object Identifier (DOI) given below. The VoR will be published online in Early View as soon as possible and may be different to this Accepted Article as a result of editing. Readers should obtain the VoR from the journal website shown below when it is published to ensure accuracy of information. The authors are responsible for the content of this Accepted Article.

To be cited as: *ChemCatChem* 10.1002/cctc.201700756

Link to VoR: <http://dx.doi.org/10.1002/cctc.201700756>

WILEY-VCH

www.chemcatchem.org



FULL PAPER

Synthesis of ZnO nanoparticles assisted by N-sources and their application in the photodegradation of organic contaminants

Gelson T. S. T. da Silva,^[a,b,#] Kele T. G. Carvalho,^[b,#] Osmando F. Lopes,^[a,b,#] Eliziana S. Gomes,^[c] Andréa R. Malagutti,^[c] Valmor R. Mastelaro,^[d] Caue Ribeiro,^{*[b]} and Henrique A. J. L. Mourão^[e]

Abstract: A modified polymeric precursor method assisted by N-sources (urea or melamine) was used to obtain anion-doped ZnO nanoparticles. The influence of these molecules on the physical-chemical and photocatalytic properties of the as-synthesized samples was investigated. The ZnO nanoparticles exhibited a hexagonal wurtzite phase and crystallite sizes of approximately 20 nm. The addition of urea or melamine to the Zn²⁺ precursor solution improved the surface properties of the materials and resulted in controlled growth of the N-doped ZnO nanoparticles, with urea showing superior performance for this purpose. These changes led to improved photocatalytic performance in the degradation of methylene blue dye and ethionamide antibiotic under UVC irradiation. It was observed that the indirect mechanism involving ·OH radical attack played the main role in both photodegradation reactions catalyzed by the as-synthesized ZnO samples, while the photosensitization mechanism had a negligible influence. The use of ESI-MS analyses showed that the MB dye molecules were broken up by the action of the ZnO photocatalyst, indicating the occurrence of a mineralization process.

Introduction

The inappropriate disposal of hazardous industrial wastes such as pesticides, dyes, and pharmaceuticals in water resources

causes serious effects in entire ecosystems, with significant impacts in the environment and to the health of living beings^[1,2]. There are increasing efforts to develop suitable processes for the elimination or reduction of such contaminants^[3-5]. Oxide semiconductors including zinc oxide (ZnO) have been successfully used in processes for the photocatalytic degradation of environmental pollutants^[6]. Their properties such as good chemical stability and suitable band gap of about 3.2 eV result in efficient photocatalysis^[7]. Several methods have been used to synthesize ZnO, such as the polymeric precursor method^[6], hydrothermal synthesis^[8], and the sol-gel method^[9]. Among these, the polymeric precursor method offers the advantages of low cost, simplicity, and controllable chemical composition, enabling good reproducibility, a high degree of crystallinity, and high purity.^[10]

Several changes in the traditional polymeric precursor method have been proposed in order to enhance the electronic, textural, and morphological properties of semiconductor materials. Abreu Jr. et al. (2005) showed that the introduction of certain additives in the polymeric resin could prevent the formation of bridge bonds between citric acid and the metallic cation, hence promoting the formation of particles with regular morphology^[11]. Various molecules have been used as sources of nitrogen or sulfur to promote doping and improve photocatalytic properties, with their degradation providing an environment rich in N or S during semiconductor crystallization^[12-14]. However, few studies have been dedicated to investigating these effects in detail. One important aspect is the effect of different molecules with similar structures in this process, since their degradation temperatures and times vary widely, enabling the control of anion doping and particle growth.

This work therefore provides a systematic investigation of the influence of the use of two different sources of N (melamine or urea) during the synthesis of ZnO nanoparticles and their effects on physical-chemical and photocatalytic properties. The photoactivity of the as-synthesized ZnO samples was probed by the degradation of methylene blue (MB) dye and ethionamide (ETA) antibiotic under ultraviolet (UVC) irradiation. Finally, a mechanism was proposed to explain the photodegradation catalyzed by the as-synthesized ZnO samples.

Results and Discussion

Characterization

As shown in Fig. 1, all the samples, with the exception of ZnO-Mel₅, exhibited similar XRD patterns in the 2θ range from 10 to 80°. These were typical of the hexagonal wurtzite ZnO structure, according to JCPDS card n° 36-1451. The results confirmed that

- [a] MSc. G.T.S.T. da Silva, Dr. O.F. Lopes
Departamento de Química
Universidade Federal de São Carlos
Rodovia Washington Luiz, km 235, 13.565-905, São Carlos, SP, Brazil
- [b] MSc. G.T.S.T. da Silva, Dr. K.T.G. Carvalho, Dr. O.F. Lopes, Dr. C. Ribeiro
Laboratório Nacional de Nanotecnologia para o Agronegócio (LNNA) - Embrapa Instrumentação
Rua XV de Novembro, n° 1452, 13.560-970, São Carlos, SP, Brazil
Tel.: +55 16 2107 2800; fax: +55 16 2107 2902.
E-mail: caue.ribeiro@embrapa.com.br
- [c] E.S. Gomes, Prof. A.R. Malagutti
Departamento de Farmácia
Universidade Federal dos Vales do Jequitinhonha e Mucuri
Rodovia MGT 367, km 583, 39.100-000, Diamantina, MG, Brazil
- [d] Prof. V.R. Mastelaro
Instituto de Física de São Carlos
Universidade de São Paulo
Avenida Trabalhador São-carlense, 400, 13566-590, São Carlos, SP, Brazil
- [e] Prof. H.A.J.L. Mourão
Instituto de Ciência e Tecnologia
Universidade Federal dos Vales do Jequitinhonha e Mucuri
Rodovia MGT 367, km 583, 39.100-000, Diamantina, MG, Brazil
- # G.T.S.T da Silva, K.T.G. Carvalho, and O.F. Lopes contributed equally to this work.

Supporting information for this article is given via a link at the end of the document.

FULL PAPER

all the products were well crystallized and revealed that the presence of urea in the Zn^{2+} resin did not significantly alter the crystalline structure or lead to the formation of any spurious phases. The same behavior was observed when smaller amounts of melamine were used during the synthesis. However, the use of 5.0 g of melamine resulted in the formation of another phase that was identified as graphitic carbon nitride ($\text{g-C}_3\text{N}_4$) (JCPDS card n° 87-1526) [15], which was the predominant phase in this sample.

The crystallite size of the ZnO phase was calculated by Scherrer's equation [16,17], using the diffraction peaks of the (100), (002), and (101) planes ($2\theta = 31.8, 34.5, \text{ and } 36.4^\circ$, respectively). As shown in Table 1, the values obtained for all the ZnO samples were very similar, with crystallite sizes of approximately 20 nm.

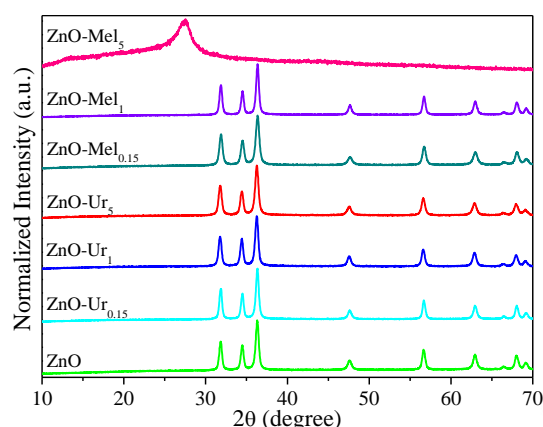


Figure 1. XRD patterns of the as-synthesized ZnO samples calcined at 550 °C.

Table 1. Crystallite size of the ZnO samples, calculated using Scherrer's equation.

Sample	Crystallite size (D_{hkl} , nm)		
	31.8° (100)	34.5° (002)	36.4° (101)
ZnO	20.6	20.8	19.6
ZnO-Ur _{0.15}	21.5	21.6	20.9
ZnO-Ur ₁	19.3	20.7	19.0
ZnO-Ur ₅	18.2	18.3	17.4
ZnO-Mel _{0.15}	18.2	17.3	17.4
ZnO-Mel ₁	22.6	10.8	20.9

The optical properties of the samples with only ZnO phase were studied by UV-visible diffuse reflectance spectroscopy. Fig. 2 shows the curves of $(\alpha h\nu)^2$ as a function of photo energy ($h\nu$), from the Tauc equation [18], for the direct band gap ZnO semiconductors [19]. The band gap energies, calculated from the x-axis intercepts of the tangent lines of the curves, were approximately 3.1–3.2 eV for all ZnO samples. The detailed results are shown in the inset of Fig. 2. In summary, the presence

of urea or melamine in the Zn^{2+} resin did not cause any significant changes in this electronic property of the as-synthesized ZnO samples.

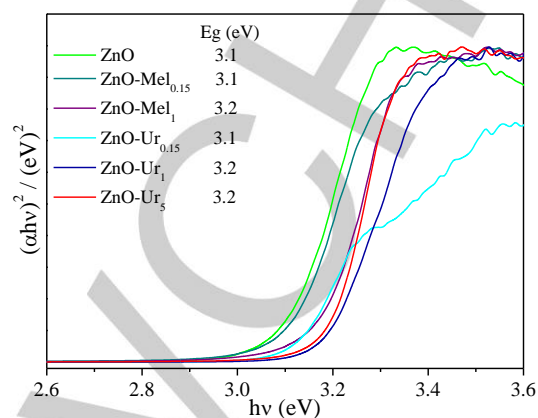


Figure 2. Tauc plot curves of the conventional ZnO, ZnO-Mel_x, and ZnO-Ur_x samples.

As shown in Fig. 3, the morphological properties of the ZnO samples were affected by the addition of the molecules of urea and melamine to the Zn^{2+} resin. The ZnO synthesized in the absence of urea and melamine consisted of rounded nanoparticles with no well-defined morphology and a broad size distribution that could be divided into two main regions with average sizes of 35 and 110 nm, as shown in Fig 3a. On the other hand, the ZnO-Mel₁ and ZnO-Ur₁ samples consisted of nanoparticles with nearly hexagonal pyramidal shapes and sizes that were more homogeneous than for the conventional ZnO sample, with average sizes of 56 and 48 nm, respectively (Fig. 3b-c). This was probably due to the presence of the amino groups in the urea and melamine molecules, which acted as complexing agents for metal ions and consequently created a physical barrier for the sintering. This provided controlled growth of the particles, resulting in a material with greater particle size homogeneity, indicating that these molecules could improve control of the particle morphology, compared to the unmodified precursor method using only citric acid as the complexing agent and ethylene glycol for polymerization.

Thermogravimetric analyses (TGA) (Fig. S1) were performed to confirm the ZnO growth mechanism. It was observed that the presence of urea or melamine led to mass losses at higher temperatures, indicating that the production of volatiles was still occurring at temperatures that typically influence particle growth. This can be clearly seen in the DTG curves, since the main mass loss peaks were at higher temperatures. Hence, this organic fraction may act to avoid contact among the particles, limiting diffusion and consequently the growth itself. However, investigation of such phenomena was not the main goal of the present work, and they are only mentioned here as an additional effect.

The morphology and structure of the as-synthesized ZnO samples were further analyzed by transmission electron

FULL PAPER

microscopy (TEM). As shown in Fig. 4, the TEM images of all the samples revealed sphere-like ZnO nanoparticles with an average size of approximately 43 nm, in good agreement with the SEM observations (Fig. 3). Therefore the particles are polycrystalline, which are composed of at least two crystallites. Furthermore, the HRTEM micrographs of the ZnO nanoparticles (Fig. 4) showed crystallites with sizes of approximately 12 nm and an average inter-fringe distance of 0.28 nm, which could be attributed to the (100) plane of the hexagonal wurtzite ZnO structure. This finding confirmed the results obtained from the XRD analysis (Fig. 1).

The chemical compositions and purities of the as-synthesized ZnO samples were further characterized by FTIR analysis. As shown in Fig. S2, the spectra exhibited similar profiles for all the ZnO samples, with absorption bands at 3445, 2923, 1634, 1386, 689, 509, and 440 cm^{-1} . All the observed absorption peaks were characteristic of a typical ZnO FTIR spectrum, without any residue of urea or melamine [20]. Bands centered at 3445 and 1634 cm^{-1} were assigned to hydroxyl groups on the ZnO surface [20,21]. A shoulder at around 2923 cm^{-1} and a small peak positioned at 1386 cm^{-1} were characteristic of $-\text{CH}_2$ stretching vibration [22], due to a small residual quantity of organic resin. A sharp and strong band in the range from 509 to 440 cm^{-1} was related to the metal-oxygen stretching mode in the ZnO lattice.

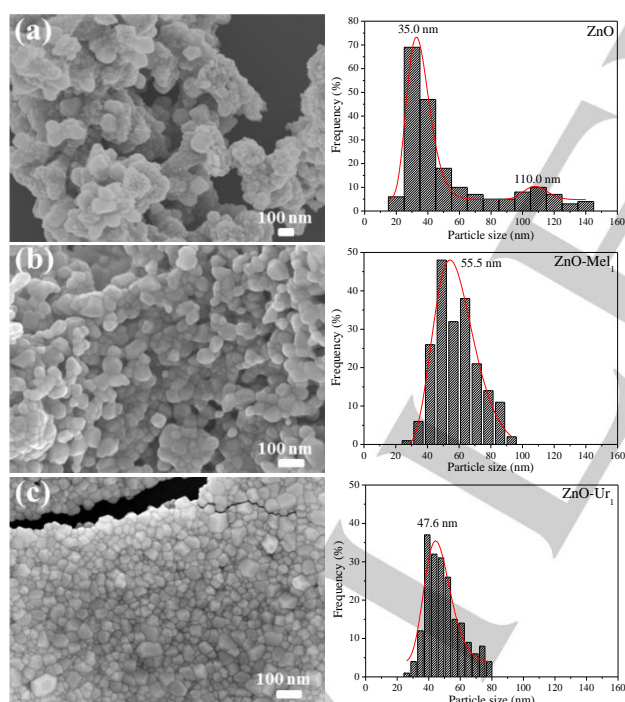


Figure 3. Representative SEM images of (a) pure ZnO, (b) ZnO-Mel₁, and (c) ZnO-Ur₁, and their respective particle size distribution histograms. The average particle size values were calculated from the lognormal distribution parameters that fitted the particle size distribution for each sample.

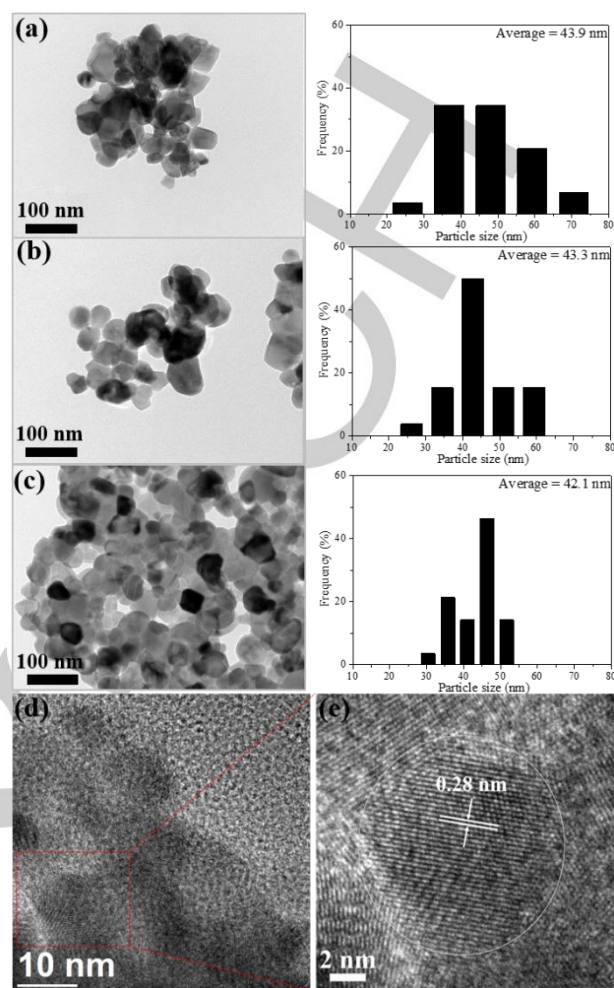


Figure 4. TEM images of the (a) ZnO, (b) ZnO-Mel₁, and (c) ZnO-Ur₁ samples, and their respective particle size distribution histograms. (d-e) HRTEM images of the ZnO.

Photocatalytic properties of the ZnO samples

The effect of adding urea and melamine molecules to the Zn²⁺ resin on the photocatalytic performance of the as-synthesized ZnO samples was evaluated using the photodegradation of MB dye under UVC irradiation (Fig. 5). All the ZnO samples were kept in contact with the MB dye solution in the dark for 12 h, in order to reach adsorption/desorption equilibrium, prior to the photocatalytic tests. It was observed that these samples exhibited negligible MB dye adsorption (<5%), and that the direct photolysis of MB dye was also insignificant.

As shown in Fig. 5, the ZnO-Mel_x and ZnO-Ur_x samples, especially ZnO-Mel₁ (Fig. 5a) and ZnO-Ur₅ (Fig. 5b), exhibited higher photocatalytic activities than the conventional ZnO. The maximum photodegradation of MB dye catalyzed by ZnO was approximately 6%, while values of 80% and 45% were obtained for the ZnO-Ur₅ and ZnO-Mel₁ samples, respectively, after 60 min of reaction. Almost complete photodegradation of the dye was achieved after 120 min using both of these samples. It could therefore be concluded that the inclusion of urea or melamine in

FULL PAPER

the ZnO synthesis significantly improved the photocatalytic properties of the as-synthesized ZnO samples. Additionally, all the ZnO-Ur_x samples showed complete MB dye decoloration after 180 min, while different behavior was observed for the ZnO-Mel_x samples. Fig. S3 shows the visible spectra and photographs showing the changes in color of the MB dye solution after different periods of the photocatalytic reaction in the absence and presence of the ZnO-Ur₅ sample.

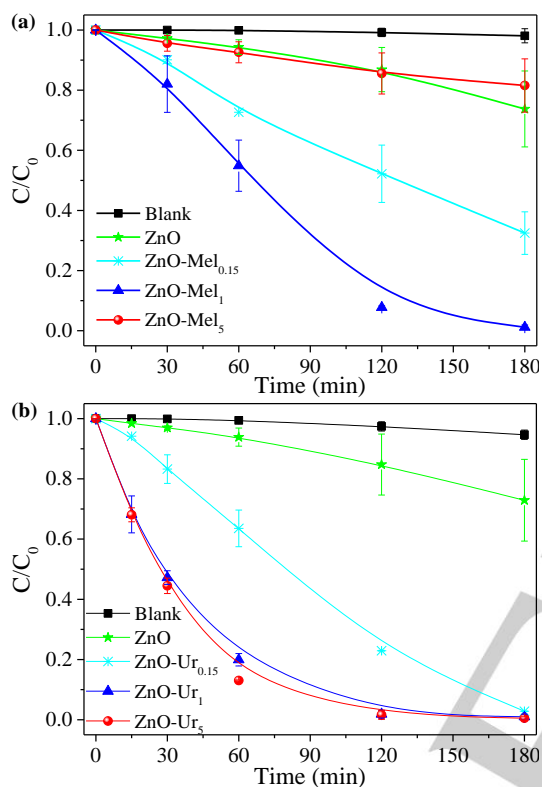


Figure 5. Kinetic curves of MB dye photodegradation catalyzed by the ZnO, ZnO-Mel_x, and ZnO-Ur_x samples under UVC irradiation. Three independent measurements were performed to estimate the standard deviation.

Similar conclusions could be reached from the reaction rate constants shown in Table 2. It was expected that the reaction kinetics should be dependent on the concentration of MB dye and the active sites of the photocatalyst. However, as the concentration of active sites remained constant throughout the degradation period, the rate law could be written as a pseudo-first order equation, as discussed in detail in our previous work^[23]. Hence, the photodegradation rate constants were obtained using the equation: $-\ln(C/C_0) = kt$, where C_0 and C_t are the concentrations of the pollutant at the start of the process and at reaction time “t”, respectively, and k is the rate constant. This analysis clearly showed that an increase in the amount of melamine in the Zn²⁺ resin from 0.15 to 1.0 g resulted in a substantial improvement in photocatalytic performance, with the rate constant obtained using ZnO-Mel₁ being approximately 4.1 times higher than with the ZnO-Mel_{0.15} sample. However, a further

increase in the amount of melamine in the Zn²⁺ resin, from 1.0 to 5.0 g, resulted in the predominant formation of g-C₃N₄ (Fig. 1), which typically exhibits the lowest photoactivity of ZnO samples under UVC irradiation. Therefore, this sample did not follow the expected trend. It should be noted that the g-C₃N₄ sample (ZnO-Mel₅) was outside the scope of this study. In the case of the ZnO-Ur_x samples, photocatalytic performance increased progressively according to the amount of urea used (ZnO-Ur_{0.15} < ZnO-Ur₁ ≤ ZnO-Ur₅), with the ZnO-Ur₅ sample presenting a rate constant approximately 2.8 times higher than obtained for ZnO-Ur_{0.15}.

The observed behavior suggested that the photocatalytic properties of the ZnO nanoparticles could be optimized by adjusting the amount of urea or melamine used in the synthesis. Also, the higher photocatalytic activities obtained for the ZnO-Ur_x samples, compared to the corresponding ZnO-Mel_x samples, indicated that urea was more effective in improving the properties of the ZnO.

Table 2. Kinetic rate constants (k_{MB}) for MB dye photodegradation.

Sample	$k_{MB} \times 10^3 \text{ (min}^{-1}\text{)}$	Sample	$k_{MB} \times 10^3 \text{ (min}^{-1}\text{)}$
Pure MB	0.1	ZnO	1.7
ZnO-Mel _{0.15}	6.3	ZnO-Ur _{0.15}	12.5
ZnO-Mel ₁	26.0	ZnO-Ur ₁	33.4
ZnO-Mel ₅	1.1	ZnO-Ur ₅	35.1

The main parameters that govern the catalytic performance of a photocatalyst are: (i) electronic properties including the band gap and lifetime of charge carriers; (ii) morphological properties involving the shape and size of the particles; and (iii) textural properties and the degree of hydroxylation and reactivity of the surface^[24–27]. In order to obtain a better understanding of the photocatalytic activities of the ZnO, ZnO-Mel₁, and ZnO-Ur₅ samples, some physical-chemical properties were further evaluated using N₂ adsorption/desorption, Fourier transform infrared spectroscopy (FTIR), and X-ray photoelectron spectroscopy (XPS).

Although the BET specific surface areas were similar for all the materials (Table 3), the mesoporous volumes of the ZnO-Ur₅ and ZnO-Mel₁ samples were approximately 2.4 and 3.0 times higher, respectively, compared to the ZnO sample, indicating enhanced access to the surface active sites of ZnO-Ur₅ and ZnO-Mel₁. This effect could have contributed to increasing the activity of the ZnO samples towards photodegradation of the MB dye.

FULL PAPER

Table 3. Textural properties of the as-synthesized ZnO samples.

Sample	SSA ^[a] (m ² ·g ⁻¹)	V _{pores} ^[b] (cm ³ ·g ⁻¹)
ZnO	10.3	0.05
ZnO-Mel ₁	8.7	0.15
ZnO-Ur ₅	7.8	0.12

[a] SSA: BET specific surface area; [b] V_{pores}: mesopore volume.

It is well known that the quantity of surface -OH groups plays an important role in photocatalytic processes [28,29], especially when the hydroxyl radical is the major active species involved in the oxidation of an organic pollutant. As discussed previously, the absorption peak at 3445 cm⁻¹ is related to the -OH surface groups and its intensity is proportional to the concentration of these groups on the surface of the material [28–30]. A semi-quantitative analysis of these groups was therefore performed for each sample (Fig. 6), with band normalization using the most intense spectrum as the reference. The ZnO-Ur₅ sample, which showed the greatest quantity of surface -OH groups, was used as the reference, and the ZnO-Mel₁ and ZnO samples presented intensities that were approximately 13% and 32% lower, respectively, compared to ZnO-Ur₅. These results were in agreement with the highest photocatalytic performance of the ZnO-Ur₅ sample.

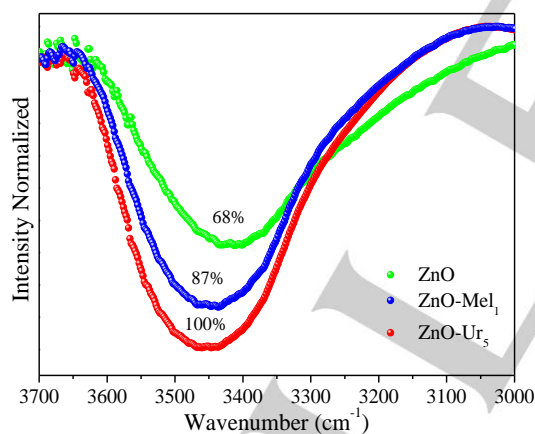


Figure 6. Normalized FTIR spectra in the -OH surface groups region (3700–3000 cm⁻¹).

XPS analysis was performed to investigate the surface composition and chemical state of the elements, and to confirm the N-doping of the ZnO-Mel₁ and ZnO-Ur₅ samples. The survey spectra of the ZnO samples (Fig. 7a) confirmed the presence of the elements Zn and O on the surfaces of all the samples, without any contamination. For all the samples, the Zn 2p XPS high-resolution spectra (Fig. 7b) showed a peak at 1022 eV related to the binding energy of Zn 2p_{3/2}. The O 1s XPS high-resolution

spectra (Fig. 7c) exhibited broad and asymmetric peaks that were deconvoluted by employing a Gaussian curve fitting to two peaks at 530.6 and 531.9 eV, attributed to the O-Zn and O-H bonds, respectively. High-resolution N 1s XPS spectra of the ZnO, ZnO-Mel₁, and ZnO-Ur₅ samples (Fig. 7d) were also collected to determine if N from urea or melamine was incorporated in the ZnO structure. As expected, no peaks related to nitrogen bonds were observed for the conventional ZnO sample. For the ZnO-Mel₁ sample, the peak attributed to nitrogen was hard to identify, due to a low signal/noise ratio. A more intense asymmetric peak at about 400 eV was observed in the N 1s XPS spectrum of the ZnO-Ur₅ sample and was fitted using two peaks at 399.5 and 400.6 eV. The peak at 399.5 eV was assigned to the Zn-N linkage resulting from the incorporation of anionic nitrogen into the ZnO crystal lattice, replacing the oxygen atoms [9,31]. The peak at 400.6 eV was attributed to oxidized nitrogen in the form of Zn-O-N or Zn-N-O linkages [13,32]. It is noteworthy that a higher intensity N 1s peak was exhibited by the ZnO-Ur₅ sample, compared to ZnO-Mel₁, indicating that the former had a greater N content. The N-doping of ZnO positively affected the electronic properties of the materials, since the ZnO-Ur₅ and ZnO-Mel₁ samples exhibited enhanced photocatalytic properties.

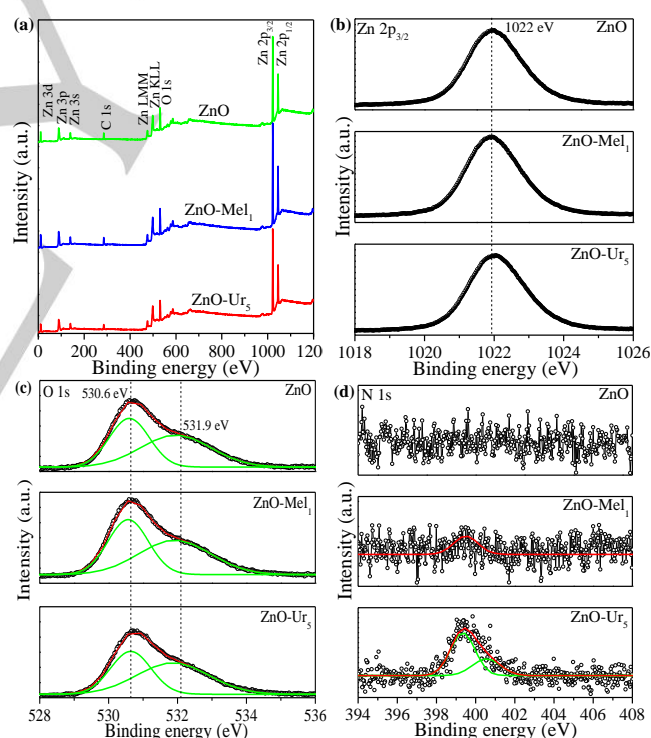


Figure 7. X-ray photoelectron spectra of the ZnO, ZnO-Mel₁, and ZnO-Ur₅ samples: survey spectra (a) and high-resolution spectra for (b) Zn 2p, (c) O 1s, and (d) N 1s.

In summary, the greater photoactivities of the ZnO-Ur_x and ZnO-Mel_x samples, compared to ZnO, were probably due to three main factors: (i) improved textural properties, associated with increased surface hydroxyl groups; (ii) smaller and more

FULL PAPER

homogeneous particles; and (iii) the incorporation of N into the ZnO lattice, which provided better electronic properties.

Study of the MB dye degradation mechanism

ZnO has been extensively used as a photocatalyst in reactions concerning the degradation of organic pollutants, artificial photosynthesis, and others [6,33]. However, only a few studies have attempted to elucidate the mechanisms of the photocatalytic reactions and identify the active species involved in the process. Therefore, investigation was made of the roles of the different mechanisms (indirect, direct, and photosensitization [26,34,35]) of the MB photodegradation under UVC irradiation, using the ZnO, ZnO-Ur₅, and ZnO-Mel₁ photocatalysts.

The contribution of the indirect mechanism ([•]OH radical formation and attack) was evaluated by determination of [•]OH using terephthalic acid (TPA) as a target molecule. The reaction between the [•]OH radical and TPA generates a fluorescent product, 2-hydroxyterephthalic acid (HTPA), which is easily monitored by the photoluminescence (PL) technique. The amount of HTPA formed is directly proportional to the quantity of [•]OH radicals generated by the irradiated photocatalyst. The PL spectra of HTPA obtained after 30 min using the as-synthesized ZnO samples under UVC irradiation are shown in Fig. 8a. The quantity of photo-generated [•]OH radicals was significantly higher when the ZnO-Ur₅ sample was used as a photocatalyst, followed by the ZnO-Mel₁ and ZnO samples. The highest amount of hydroxyl radicals generated by the ZnO-Ur₅ sample was due to its improved electronic structure, as well as the large quantity of hydroxyl groups on its surface.

The reaction between TPA and the [•]OH radical is only dependent on diffusion of the [•]OH radicals in the solution, so the quantity of photo-generated [•]OH radicals is directly proportional to the amount of HTPA formed. Hence, the kinetic constants for formation of HTPA and [•]OH radicals are similar [29,36–38], so the rate constant for [•]OH radical (k_{OH}) generation could be obtained by applying the pseudo-zero order reaction equation to the HTPA formation data (Fig. 8b). The highest rate constant was found for the ZnO-Ur₅ sample, followed by the ZnO-Mel₁ and ZnO samples. Therefore, the rate constants for [•]OH radical formation and for organic pollutants photodegradation, both catalyzed by the as-synthesized ZnO samples, exhibited the same trend (Fig. S4). These results strongly indicated that the indirect mechanism played a major role in the photodegradation process, since the order of [•]OH radical formation followed the order of photoactivity for the ZnO samples.

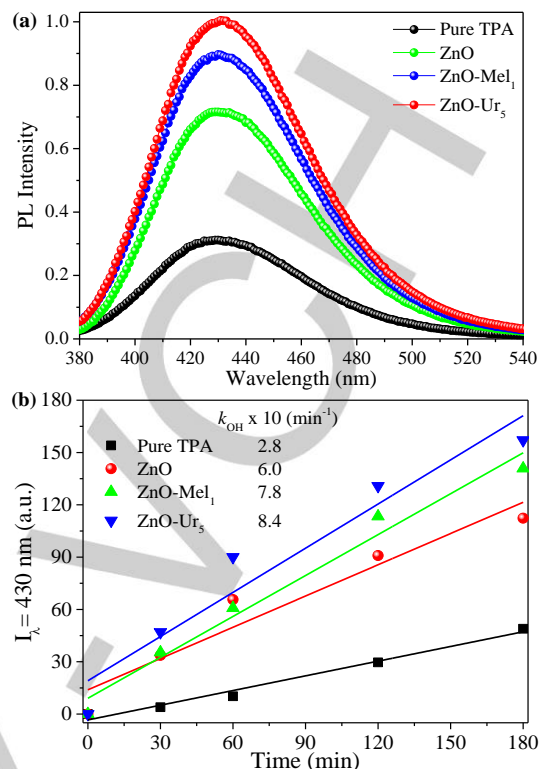


Figure 8. (a) PL spectra for 2-hydroxyterephthalic acid formation after 30 min under UVC irradiation, using the ZnO, ZnO-Mel₁, and ZnO-Ur₅ photocatalysts. (b) Pseudo-zero order kinetics for indirect formation of hydroxyl radicals by the samples.

The photo-oxidation of the MB dye molecules catalyzed by the ZnO-Ur₅ sample was confirmed by analysis of the MB solution using electrospray ionization mass spectrometry (ESI-MS). The ESI-MS spectrum for the MB dye standard solution (Fig. 9a) only exhibited a strong signal at a mass/charge (m/z) ratio of 284, attributed to the MB structure without any oxidation. After 120 min of UVC irradiation in the presence of the ZnO-Ur₅ photocatalyst, the ESI-MS spectrum for the MB dye solution (Fig. 9b) exhibited several peaks at m/z 332, 318, 301, 284, 270, 256, 243, 162, and 129. Furthermore, the intensity of the signal at m/z 284 was lower than in the spectrum for pure MB dye, indicating a decrease in its proportion following the formation of other species. The signals at m/z 301, 318, and 332 reflected successive hydroxylation in the aromatic ring of the MB molecule, confirming that the [•]OH radical played an important role in the MB dye photodegradation reaction, under the conditions used. The signals at m/z 270, 256, and 243 reflected the loss of one or more methyl substituents from the amine groups of MB, forming the azure B, azure A, and azure C species, respectively [39]. Additionally, signals at m/z 129 and 162 corresponded to cleavage of the aromatic ring due to attack by active species that were photogenerated in the presence of the ZnO-Ur₅ sample under UVC irradiation. It should be noted that this last finding confirmed that the MB dye molecules were broken down using the photocatalyst, which was strongly indicative of the occurrence of a mineralization process. This finding was very important, because a good catalyst must be able to break down

FULL PAPER

the contaminant molecule, while at the same time minimizing the possible formation of by-products that could also be toxic. Based on the ESI-MS results, a schematic diagram (Fig. S5) was proposed to clearly describe the mechanism of the MB dye photodegradation catalyzed by the as-synthesized ZnO samples.

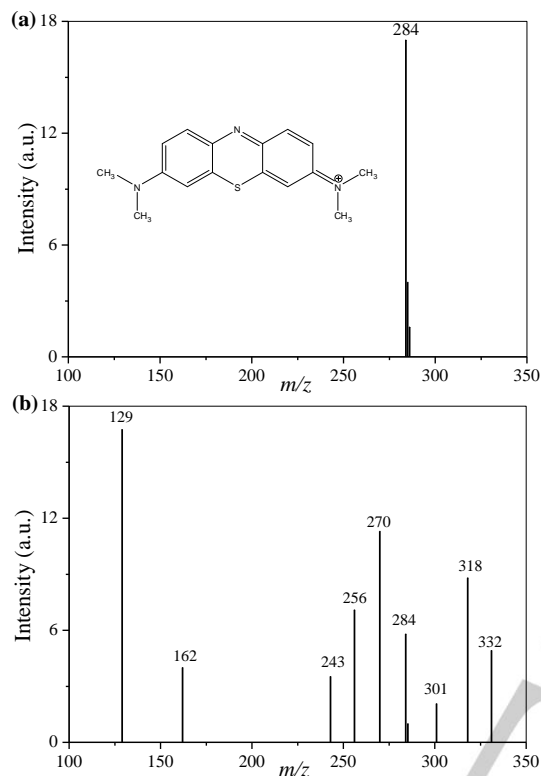


Figure 9. ESI mass spectra of (a) pure MB dye and (b) MB dye after photodegradation catalyzed by the ZnO-Ur₅ sample during 120 min under UVC irradiation.

The stability of a photocatalyst is a crucial parameter in catalytic applications such as the treatment of wastewater [40]. Therefore, the photostability of the pure ZnO and ZnO-Ur₅ samples was evaluated by performing recycling experiments for 180 min under UVC irradiation. As shown in Fig. 10, no significant deactivation (<5%) was observed for both photocatalysts, even after four successive re-uses for MB dye photodegradation.

The structural, electronic, and morphological properties of the ZnO-Ur₅ photocatalyst were analyzed by the XRD, UV-vis DRS, and SEM techniques, before and after MB dye degradation for 180 min under UVC irradiation. There were no significant changes in the XRD pattern or the SEM image of the used ZnO-Ur₅ sample, compared to the fresh material (Fig. S6). The band gap value of the used sample showed a slight increase, from 3.15 to 3.21 eV, which could be attributed to experimental error. These results revealed that the photocatalyst exhibited high structural, electronic, and morphological stability during the photocatalytic reaction, under the conditions employed.

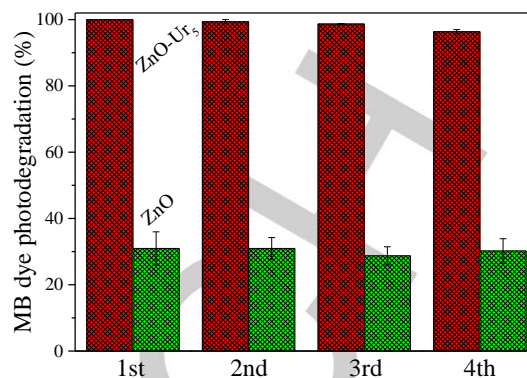


Figure 10. Stability of the pure ZnO and ZnO-Ur₅ photocatalysts during four cycles of MB dye photodegradation.

Photodegradation of ethionamide (ETA) antibiotic

Ethionamide (ETA), a first-line antibiotic used for the treatment of tuberculosis, was employed here as a model of a real organic pollutant, with maximum absorption centered at 289 nm in the ultraviolet region (Fig. S7) [41]. Fig. 11a shows the kinetic curves for ETA photodegradation catalyzed by the as-synthesized ZnO samples under UVC irradiation. The photodegradation curves linearized by pseudo-first order kinetics are shown in Fig. 11b, and the rate constant (k_{ETA}) values are provided in the inset of Fig. 11b. All the as-synthesized ZnO samples exhibited ETA photodegradation activity, negligible ETA adsorption (<5%), and the direct photolysis of this molecule was insignificant. The k_{ETA} values calculated for ETA degradation in the presence of the ZnO-Ur₅ and ZnO-Mel₁ photocatalysts were approximately 3.7 and 2.2 times higher, respectively, compared to the value obtained for conventional ZnO. The ratio of the effectiveness of these samples was the same as for MB dye photodegradation (k_{MB}) and for $\cdot\text{OH}$ radical generation ($k_{\text{OH}\cdot}$), indicating that the main degradation mechanism was also due to the attack of hydroxyl radicals on the ETA molecules. Thus, these results suggested that photosensitization was not the main factor responsible for photodegradation of the studied organic pollutants (MB and ETA) catalyzed by the as-synthesized ZnO samples, and that the degradation process was independent of the target molecule. The main mechanism for photodegradation of the molecules was by the direct action of hydroxyl radicals, as discussed previously. These radicals are highly reactive and non-selective, which makes the process independent of the molecule to be degraded. In summary, the as-synthesized ZnO photocatalysts exhibited excellent potential for application in real photocatalytic processes to degrade any type of organic pollutant. Table S1 provides a comparison of the photoactivities of different photocatalysts and ZnO-Ur₅ for MB dye degradation under identical experimental conditions (i.e., light source, photocatalyst amount, MB dye concentration, and reactor design). This comparison demonstrates the excellent performance of ZnO-Ur₅.

FULL PAPER

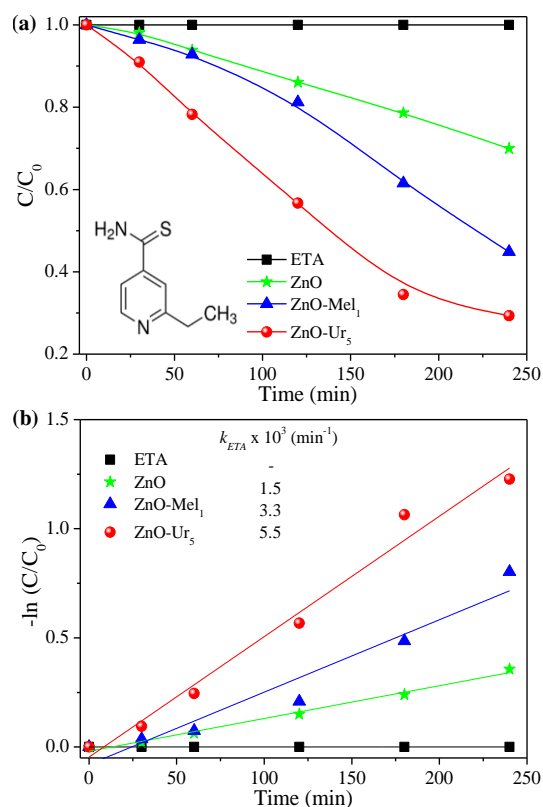


Figure 11. (a) Kinetic curves of ethionamide photodegradation catalyzed by the ZnO, ZnO-Mel₁, and ZnO-Ur₅ samples under UVC irradiation. (b) First order kinetics of ethionamide degradation catalyzed by the as-synthesized samples.

Conclusions

In summary, it was found that ZnO samples prepared using a modified polymeric precursor method with addition of urea (ZnO-Ur_x) or melamine (ZnO-Mel_x) exhibited higher photocatalytic efficiencies for degradation of organic pollutants, compared to ZnO obtained conventionally. The use of these molecules (melamine and urea) in the synthesis provided controlled growth of the ZnO particles, resulting in materials with more homogeneous particle sizes. The as-synthesized ZnO-Ur_x and ZnO-Mel_x samples showed enhanced performance in the degradation of MB dye and ETA antibiotic, which are derived from industrial and domestic sources and are potential contaminants in water. The greater quantity of surface hydroxyl groups, the incorporation of nitrogen into the ZnO lattice, and the enhanced textural properties of the materials could explain the improved photoactivity of these samples. These positive effects were most pronounced in the case of the ZnO-Ur_x samples. Investigation of the photocatalysis mechanism showed that degradation of the pollutants over all the photocatalysts proceeded mainly by means of non-selective $\cdot\text{OH}$ radical attack, and that the photosensitization mechanism exerted a negligible effect. Additionally, the results of ESI-MS analysis demonstrated that the MB dye molecules were oxidized by the action of the ZnO photocatalyst, which was indicative of a mineralization process.

Experimental Section

Reagents

The chemicals used were zinc acetate ($\text{Zn}(\text{CH}_3\text{COO})_2 \cdot 2\text{H}_2\text{O}$, ≥ 98 wt.%, Synth), citric acid ($\text{HOC}(\text{CO}_2\text{H})(\text{CH}_2\text{CO}_2\text{H})_2$, > 99 wt.%, Quemis), ethanol ($\text{CH}_3\text{CH}_2\text{OH}$, ≥ 99.5 wt.%, Quemis), ethylene glycol ($\text{HOCH}_2\text{CH}_2\text{OH}$, > 99 wt.%, Synth), nitric acid (HNO_3 , Exodo Cientifica), melamine ($\text{C}_3\text{N}_6\text{H}_6$, 99 wt.%, Sigma-Aldrich), urea ($\text{CH}_4\text{N}_2\text{O}$, > 99 wt.%, Synth), methylene blue ($\text{C}_{16}\text{H}_{18}\text{N}_3\text{S}$, Vetec), ethionamide ($\text{C}_8\text{H}_{10}\text{N}_2\text{S}$, 98 wt.%, Sigma-Aldrich), sodium hydroxide (NaOH , Synth), and terephthalic acid ($\text{C}_6\text{H}_4(\text{COOH})_2$, 98 wt.%, Aldrich). All reagents were used as received, without further purification.

Synthesis of materials

The polymeric citrate precursor method was used to synthesize the ZnO samples. In a typical procedure, 5 g (0.023 mol) of zinc acetate and 13 g (0.068 mol) of citric acid were dissolved in 200 mL (3.43 mol) of ethanol and 8 mL (0.143 mol) of ethylene glycol at 70 °C. Then, 6 mL of HNO_3 was added to the mixture to complete dissolution. The volume of the solution obtained was reduced by evaporation using a hotplate at 90 °C for 30 min, under magnetic stirring, resulting in a viscosity of approximately 5.5 cP. This resulted solution was referred as Zn^{2+} resin. Finally, seven ZnO samples were obtained by heat treatment of Zn^{2+} resin in an electric furnace, using the following parameters: heating at a rate of 2 °C·min⁻¹ until 100 °C and holding at this temperature for 1 h; heating at 3 °C·min⁻¹ until 300 °C and holding at this temperature for 2 h to remove the organic portion; and heating at 3 °C·min⁻¹ until 550 °C and holding at this temperature for 2 h to obtain fully crystallized ZnO nanoparticles. A conventional ZnO sample (referred to as ZnO) was obtained from 11 mL of pure Zn^{2+} resin. Another six samples were obtained by adding different weight amounts of melamine (Mel) or urea (Ur), i.e. 0.15 g, 1.0 g, and 5.0 g, to 11 mL of Zn^{2+} resin. These samples are referred to as ZnO-Mel_x or ZnO-Ur_x, where x is the weight of added Mel or Ur molecules.

Characterization

X-ray diffraction (XRD) measurements were carried out with a Shimadzu XRD 6000 diffractometer, using nickel-filtered $\text{Cu K}\alpha$ radiation, 2 θ from 10° to 80° in continuous scanning mode, and a step width of 0.02°. UV-Vis diffuse reflectance spectra (DRS) were recorded from 200 to 800 nm using a Shimadzu UV-2600 spectrophotometer equipped with an integrating sphere (ISR-2600 Plus). Magnesium oxide (MgO) powder was used as a reflectance standard. Fourier transform infrared (FTIR) spectra were recorded from 4000 to 500 cm⁻¹ using a Bruker Vertex 70 spectrophotometer, with a resolution of 4 cm⁻¹ and averaging of 32 scans. The samples were mixed with potassium bromide in a mass ratio of 1:100 (ZnO:KBr) and then pressed to form thin discs. Scanning electron microscopy (SEM) images were obtained with a JEOL JSM-6701F field emission instrument. Transmission electron microscopy (TEM) images were obtained with a FEI Tecnai G2 F20 microscope operated at 200 kV. Thermogravimetric analyses (TGA) were performed on a Shimadzu TGA-50 equipment using oxidative atmosphere conditions (air flow rate of 60 mL·min⁻¹), temperature range from 30 to 600 °C and heating rate of 10 °C·min⁻¹. Specific surface area (SSA) values were calculated according to the Brunauer-Emmett-Teller (BET) method, using N₂ adsorption data obtained at -196 °C with a Micromeritics ASAP-2020 system. Samples were previously treated (degassed) by heating at 80 °C under vacuum until reaching a degassing pressure lower than 20 $\mu\text{m Hg}$. X-ray photoelectron spectroscopy (XPS) was performed using a ScientaOmicron ESCA+ spectrometer with a high performance hemispheric analyzer (EA 125), using monochromatic Al K α ($h\nu = 1486.6$ eV) radiation as the excitation source. The operating pressure in the ultra-high vacuum (UHV) chamber during the analysis was 2×10^{-9} mbar. Energy steps of 50 and 20 eV were

FULL PAPER

used for the survey and high resolution spectra, respectively. The following peaks were used for the quantitative analysis: O 1s, C 1s, N 1s, and Zn 2p. The C–(C, H) component of the C1s peak of adventitious carbon was fixed at 284.5 eV to set the bond energy scale, and treatment of the data employed CasaXPS software.

Photocatalytic tests

The photoactivity of the ZnO samples was evaluated in the degradation of methylene blue (MB) dye under ultraviolet (UVC) irradiation. In a typical procedure, 10 mg of photocatalyst was placed in contact with 20 mL of an aqueous solution of MB (10 mg·L⁻¹). All the experiments employed a photoreactor^[37] equipped with six UVC lamps (Philips TUV, 15 W, maximum emission at 254 nm and average light intensity of 40 W·m⁻²; see the spectral distribution in Fig. S8), a magnetic stirrer, and a heat exchanger that maintained the temperature at 18 °C. The photodegradation of the MB dye was monitored at regular intervals using a Shimadzu UV-1601 PC spectrophotometer in the visible range, since this molecule exhibits maximum absorbance at 654 nm. Before the kinetic experiments, the suspensions were kept in the dark for 12 h in order to establish adsorption/desorption equilibrium of the dye on the photocatalyst surface. The same conditions were used to evaluate the activity of the as-synthesized ZnO samples in degradation of ethionamide antibiotic (2-ethylpyridine-4-carbothioamide, ETA). The initial concentration of ETA was 10 mg·L⁻¹ and its decreasing concentration was monitored at 289 nm.

Mass spectrometry (MS) was employed to elucidate the mechanism of oxidation of MB dye and the formation of byproducts during the photocatalytic process, using the ZnO sample with the highest activity. The solutions were monitored using electrospray ionization mass spectrometry (ESI-MS, Varian 310-MS), in positive ion mode. Aliquots were introduced into the ESI source using a syringe pump and a flow of N₂ was maintained at 20 mL·min⁻¹. The products are referred to using the *m/z* ratio of the protonated molecular ion.

Hydroxyl radical formation tests

The ability of each ZnO photocatalyst to form hydroxyl radicals (·OH) under UVC irradiation was indirectly determined by the photoluminescence technique, using terephthalic acid (TPA) as the target molecule^[29,36,37]. The reaction between photo-generated ·OH radicals and TPA results in the formation of 2-hydroxyterephthalic acid (HTPA), which is fluorescent^[29,36,37]. Hence, the HTPA concentration is proportional to the ·OH radical concentration. In these experiments, 10 mg of ZnO photocatalyst was placed in contact with 20 mL of a solution of TPA (5×10⁻⁴ mol·L⁻¹) prepared in aqueous NaOH (2×10⁻³ mol·L⁻¹). All experiments were carried out using the photoreactor described previously in Section 2.3. At regular intervals, the HTPA concentration was monitored by fluorescence measurements using a Shimadzu RF-5301PC spectrofluorophotometer. The fluorescence emission spectrum in the wavelength range from 380 to 540 nm ($\lambda_{\text{maximum}} = 430$ nm) was obtained using excitation at 315 nm.

Acknowledgements

The authors are grateful to the Ministry of Science, Technology, and Innovation (through SisNANO Program - National System of Laboratories in Nanotechnology), the National Council for Scientific and Technological Development (CNPq, grant #300247/2013-3, #402.287/2013-4, and #454438/2014-1), Coordination for the Improvement of Higher Education Personnel (CAPES), Sao Paulo Research Foundation (FAPESP, grants #13/13888-0, #15/12304-0, and #16/09746-3), and Embrapa Rede AgroNano for their financial support. The authors also thank

Prof. Dr. Waldir Avansi Jr. and FAPESP (grant #13/17639-4) for providing DRS spectroscopy facilities.

Keywords: zinc oxide • polymeric precursor method • photocatalysis • water decontamination

- [1] M. Chen, W. Chu, *J. Hazard. Mater.* **2012**, 219-220, 183–189.
- [2] H. Dong, G. Chen, J. Sun, C. Li, Y. Yu, D. Chen, *Appl. Catal. B, Environ.* **2013**, 134-135, 46–54.
- [3] C. Li, G. Chen, J. Sun, J. Rao, Z. Han, Y. Hu, W. Xing, C. Zhang, *Appl. Catal. B Environ.* **2016**, 188, 39–47.
- [4] C. Li, G. Chen, J. Sun, H. Dong, Y. Wang, C. Lv, *Appl. Catal. B Environ.* **2014**, 160-161, 383–389.
- [5] G. T. S. T. da Silva, K. T. G. Carvalho, O. F. Lopes, C. Ribeiro, *Appl. Catal. B, Environ.* **2017**, 216, 70–79.
- [6] K. T. G. Carvalho, S. C. Fidelis, O. F. Lopes, C. Ribeiro, *Ceram. Int.* **2015**, 41, 10587–10594.
- [7] K. M. Lee, C. W. Lai, K. S. Ngai, J. C. Juan, *Water Res.* **2016**, 88, 428–448.
- [8] J. Yu, X. Yu, *Environ. Sci. Technol.* **2008**, 42, 4902–4907.
- [9] J. J. Macías-Sánchez, L. Hinojosa-Reyes, A. Caballero-Quintero, W. de la Cruz, E. Ruiz-Ruiz, A. Hernández-Ramírez, J. L. Guzmán-Mar, *Photochem. Photobiol. Sci.* **2015**, 14, 536–42.
- [10] N. L. V. Carreño, L. Edson R, L. P. S. Santos, P. N. Lisboa-Filho, E. Longo, G. C. L. Araújo, A. Barison, A. G. Ferreira, A. Valentini, L. F. D. Probst, *Quim. Nova* **2002**, 25, 935–942.
- [11] A. Jr., S. M. Zanetti, M. A. S. Oliveira, G. P. Thim, *J. Eur. Ceram. Soc.* **2005**, 25, 743–748.
- [12] N. P. Herring, L. S. Panchakarla, M. S. El-Shall, *Langmuir* **2014**, 30, 2230–2240.
- [13] I. M. P. Silva, G. Byzinski, C. Ribeiro, E. Longo, *J. Mol. Catal. A Chem.* **2016**, 417, 89–100.
- [14] J. J. L. Hmar, T. Majumder, S. Dhar, S. P. Mondal, *Thin Solid Films* **2016**, 612, 274–283.
- [15] H. Yiming, Y. Wang, L. Zhang, B. Teng, M. Fan, *Appl. Catal. B Environ.* **2015**, 168, 1–8.
- [16] A. L. Patterson, *Phys. Rev.* **1939**, 15, 978–981.
- [17] J. I. Langford, a. J. C. Wilson, *J. Appl. Crystallogr.* **1978**, 11, 102–113.
- [18] J. Tauc, *Mater. Res. Bull.* **1970**, 5, 721–730.
- [19] S. Anandan, N. Ohashi, M. Miyauchi, *Appl. Catal. B Environ.* **2010**, 100, 502–509.
- [20] Z. Dai, K. Liu, Y. Tang, X. Yang, J. Bao, J. Shen, *J. Mater. Chem.* **2008**, 18, 1919.
- [21] J. Singh, P. Kumar, K. S. Hui, K. N. Hui, K. Ramam, R. S. Tiwari, O. N. Srivastava, *CrystEngComm* **2012**, 14, 5898.
- [22] Y. Chen, H. Zhao, B. Liu, H. Yang, *Appl. Catal. B Environ.* **2015**, 163, 189–197.
- [23] V. R. de Mendonça, H. A. J. L. Mourão, A. R. Malagutti, C. Ribeiro, *Photochem. Photobiol.* **2014**, 90, 66–72.
- [24] H. A. J. L. Mourão, V. R. de Mendonça, A. R. Malagutti, C. Ribeiro, *Quim. Nova* **2009**, 32, 2181–2190.
- [25] O. F. Lopes, V. R. De Mendonça, F. B. F. Silva, E. C. Paris, C. Ribeiro, *Quim. Nova* **2014**, 38, 106–117.

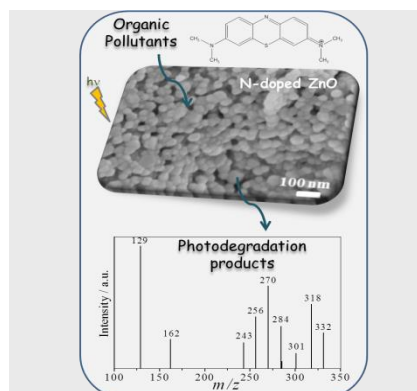
FULL PAPER

- [26] M. A. Henderson, *Surf. Sci. Rep.* **2011**, *66*, 185–297.
- [27] U. I. Gaya, A. H. Abdullah, *J. Photochem. Photobiol. C Photochem. Rev.* **2008**, *9*, 1–12.
- [28] V. R. de Mendonça, O. F. Lopes, R. P. Fregonesi, T. R. Giraldo, C. Ribeiro, *Appl. Surf. Sci.* **2014**, *298*, 182–191.
- [29] O. F. Lopes, E. C. Paris, C. Ribeiro, *Appl. Catal. B Environ.* **2014**, *144*, 800–808.
- [30] J. Bertaux, F. Froehlich, P. Ildefonse, *J. Sediment. Res.* **1998**, *68*, 440–447.
- [31] M. Wang, F. Ren, J. Zhou, G. Cai, L. Cai, Y. Hu, D. Wang, Y. Liu, L. Guo, S. Shen, *Sci. Rep.* **2015**, *5*, 12925.
- [32] S. A. Bakar, G. Byzinski, C. Ribeiro, *J. Alloys Compd.* **2016**, *666*, 38–49.
- [33] Y. He, Y. Wang, L. Zhang, B. Teng, M. Fan, *Appl. Catal. B Environ.* **2015**, *168*, 1–8.
- [34] Y. Mao, C. Schoeneich, K. Asmus, *J. Phys. Chem.* **1991**, *95*, 10080–10089.
- [35] K. Ishibashi, A. Fujishima, *J. Photochem. Photobiol. A Chem.* **2000**, *134*, 139–142.
- [36] K. Ishibashi, A. Fujishima, T. Watanabe, K. Hashimoto, *Electrochem. Commun.* **2000**, *2*, 207–210.
- [37] O. F. Lopes, K. T. G. Carvalho, G. K. Macedo, V. R. de Mendonça, W. Avansi, C. Ribeiro, *New J. Chem.* **2015**, *39*, 6231–6237.
- [38] O. F. Lopes, K. T. G. Carvalho, A. E. Nogueira, W. Avansi, C. Ribeiro, *Appl. Catal. B Environ.* **2016**, *188*, 87–97.
- [39] A. Petzer, B. H. Harvey, G. Wegener, J. P. Petzer, *Toxicol. Appl. Pharmacol.* **2012**, *258*, 403–409.
- [40] V. A. Online, H. Dong, G. Chen, J. Sun, Y. Feng, C. Li, C. Lv, *Chem. Commun.* **2014**, *50*, 6596–6599.
- [41] B. R. L. Ferraz, F. R. F. Leite, B. L. Batista, M. Andréa R, *Bioelectrochemistry* **2012**, *88*, 36–41.

FULL PAPER

FULL PAPER

N-doped ZnO nanoparticles were obtained by an easy method assisted by urea or melamine molecules, which improved the physical-chemical properties of ZnO. Modified ZnO showed high photoactivity for degradation of methylene blue dye and ethionamide antibiotic. The mechanism of pollutants photodegradation catalyzed by as-synthesized ZnO is proposed.



Gelson T. S. T. da Silva, Kele T. G. Carvalho, Osmando F. Lopes, Eliziana S. Gomes, Andréa R. Malagutti, Valmor R. Mastelaro, Caue Ribeiro,* and Henrique A. J. L. Mourão

Page No. – Page No.

Synthesis of ZnO nanoparticles assisted by N-sources and their application in the photodegradation of organic contaminants